

# A New Class of Mirrors for Wide-Angle Imaging

Mandyam V. Srinivasan

Centre for Visual Sciences, Research School of Biological Sciences, Australian National University,  
PO Box 475, Canberra, ACT 2601, Australia

## Abstract

*Conventional mirrors for panoramic imaging usually capture circular images. As these images are difficult to interpret visually, they are often remapped digitally into a rectangular image in which one axis represents azimuth and the other elevation. This paper describes a class of mirrors that perform the capture as well as the remapping, thus eliminating the need for computational resources. They provide uniform resolution in azimuth and elevation, and can be designed to make full use of a camera's imaging surface.*

## Introduction

Over the past five years or so there has been considerable interest in the design and development of reflective surfaces for panoramic imaging. Such surfaces can be used in a variety of applications including surveillance, security, robotics, video conferencing, web-based advertising and tourism. Reflective surfaces are often more suitable for such applications than conventional wide-angle lenses because the former are lighter, less expensive and cover a greater field of view. In addition, as we shall see below, reflective surfaces can be readily tailored to image the environment in a variety of prescribed ways.

The most common class of reflective mirrors used for panoramic imaging consists of a mirror in the shape of a generalized cone. The camera, aligned along the optical axis of the cone, captures a circular image of the environment, in which the radial distance of a pixel from the center of the image is a function of the angle of elevation of the point in the environment that it represents, and the azimuthal direction of the pixel corresponds to the azimuthal bearing of this point.

Mirrors of this kind have been designed to suit a variety of specific requirements, such as (i) ensuring that the effective point from which the environment is viewed is constant, independent of the elevation or the azimuth of the viewing direction [1]; (ii) ensuring that pixel resolution of elevation is constant, irrespective of the direction of view [2, 3]; and (iii) using a combination of refractive and reflective optics to achieve requirement (i) [4].

While this class of mirrors is very effective in imaging large sections of the environment, the circular images that they capture are difficult to interpret by the human visual system. To facilitate visualization, the image must be digitally re-mapped, or “unwarped”, to

produce a rectangular image in which the abscissa represents azimuth, for example, and the ordinate elevation. The unwarped image is more amenable to inspection, interpretation and understanding of the scene. However, the unwarping requires computational resources.

A few studies have explored the design of mirrors that achieve wide-angle image capture as well as unwarping, optically. One study presents a mirror design for imaging a fronto-parallel plane in this way [5]. Another achieves a mapping of a limited section of the environment in elevation and azimuth [6].

Here we describe a new class of mirrors that map large sections of the environment and produce readily interpretable, rectangular images of the environment in coordinates of azimuth and elevation. The mirrors achieve wide-angle image capture as well as unwarping, thus eliminating the need to use a computer for the unwarping process.

## Organization of the paper

This paper is structured as follows. First, we present the theory underlying the derivation of the mirror profiles. We then consider two classes of mirror profiles: one in which the optical axis of the camera is in the equatorial plane of the viewsphere, and another in which the optical axis is aligned with the poles of the viewsphere. An example of the profile of a mirror in each class is shown and its performance is illustrated in a ray-tracing environment. The paper concludes with a brief discussion of the advantages and disadvantages of these mirrors.

## Calculation of mirror profile

The theory underlying the calculation of the mirror profiles is described below.

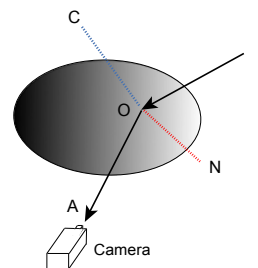


*Fig. 1 Illustration of reflection geometry*

Fig. 1 shows a ray BO from the external environment impinging on the mirror, and the reflected ray OA entering the camera. The mapping properties of the required mirror specify the relationship between the directions of the

incident and reflected rays. Given this constraint, the local orientation of the mirror surface must be such that the incident ray is reflected into the camera. For this to occur, the reflected ray must (a) lie in the plane containing the incident ray and the normal (ON) to the surface at the point of reflection; and (b) the surface normal must bisect the angle between the incident and reflected rays. We denote the direction cosines (d.c.'s) of the ray entering the camera by  $(a_x, a_y, a_z)$ . For any point  $(x, y, z)$  on the mirror surface, these d.c.'s are given by

$$a_x = \frac{-x}{\sqrt{x^2 + y^2 + z^2}} \quad (1)$$

$$a_y = \frac{-y}{\sqrt{x^2 + y^2 + z^2}} \quad (2)$$

and

$$a_z = \frac{z}{\sqrt{x^2 + y^2 + z^2}} \quad (3)$$

where the origin of the co-ordinate system is at the nodal point of the camera.

We denote the d.c.'s of the reversed direction of the ray impinging on the mirror by  $(b_x, b_y, b_z)$ . We represent the surface profile by the function  $f = z + q(x, y) = 0$ . It is well known [7] that the d.c.'s of the normal to a surface defined by  $f$

are proportional to  $\frac{\partial f}{\partial x}$ ,  $\frac{\partial f}{\partial y}$  and  $\frac{\partial f}{\partial z}$  (where

$\frac{\partial f}{\partial z} = 1$ ). We denote these partial derivatives by

$(p_x, p_y, p_z)$ .

In order to satisfy constraint (a) above, let us first calculate the d.c.'s of a line OC that is perpendicular to OA as well as ON. Denoting the d.c.'s of OC by  $(c_x, c_y, c_z)$ , we have

$$c_x \cdot a_x + c_y \cdot a_y + c_z \cdot a_z = 0 \quad (4)$$

and

$$c_x \cdot p_x + c_y \cdot p_y + c_z \cdot p_z = 0 \quad (5)$$

Setting  $p_z = 1$  and solving for  $c_x$  and  $c_y$ , we obtain

$$c_x = c_z \frac{(p_y \cdot a_z - a_y)}{(p_x \cdot a_y - a_x \cdot p_y)} \quad (6)$$

and

$$c_y = c_z \frac{(a_x - p_x \cdot a_z)}{(p_x \cdot a_y - a_x \cdot p_y)} \quad (7)$$

Constraint (a) requires that OB be perpendicular to OC. This implies that

$$c_x \cdot b_x + c_y \cdot b_y + c_z \cdot b_z = 0 \quad (8)$$

Substituting for  $c_x$  and  $c_y$  from (6) and (7) into (8), we obtain

$$p_x \cdot (b_z \cdot a_y - a_z \cdot b_y) + p_y \cdot (b_x \cdot a_z - b_z \cdot a_x) = b_x \cdot a_y - a_x \cdot b_y \quad (9)$$

To satisfy constraint (b), we require that the angle between ON and OA be equal to that between ON and OB. This requires that

$$a_x \cdot p_x + a_y \cdot p_y + a_z \cdot p_z = b_x \cdot p_x + b_y \cdot p_y + b_z \cdot p_z \quad (10)$$

which, after setting  $p_z = 1$ , may be rewritten as

$$p_x \cdot (b_x - a_x) + p_y \cdot (b_y - a_y) + (b_z - a_z) = 0 \quad (11)$$

Solving for  $p_x$  and  $p_y$  from (9) and (11), we obtain

$$p_x = \frac{\partial f}{\partial x} = \frac{(b_y - a_y) \cdot (b_x \cdot a_y - a_x \cdot b_y) + (a_z - b_z) \cdot (a_x \cdot b_z - a_z \cdot b_x)}{(b_y - a_y) \cdot (b_z \cdot a_y - a_z \cdot b_y) + (a_x - b_x) \cdot (b_x \cdot a_z - b_z \cdot a_x)} \quad (12)$$

$$p_y = \frac{\partial f}{\partial y} = \frac{(a_x - b_x) \cdot (b_x \cdot a_y - a_x \cdot b_y) + (a_z - b_z) \cdot (b_z \cdot a_y - a_z \cdot b_y)}{(b_y - a_y) \cdot (b_z \cdot a_y - a_z \cdot b_y) + (a_x - b_x) \cdot (b_x \cdot a_z - b_z \cdot a_x)} \quad (13)$$

and

$$p_z = \frac{\partial f}{\partial z} = 1 \quad (14)$$

We now consider two classes of mirrors: (A) Equatorial view mirrors and (B) Polar view mirrors.

### A. Equatorial view mirrors

The configuration of an equatorial view mirror is illustrated in Fig. 2. The figure shows the mirror surface, the nodal point of the camera, and the camera's image plane (which is drawn in front of the nodal point, for simplicity, rather than behind it). The mapping we desire is one in which the optical axis of the camera is in the equatorial plane of the viewsphere. Points of constant elevation ( $\phi_0$ ) in the outside world map to horizontal lines in the image plane. These horizontal lines represent lines of constant  $\phi$  in the camera (Fig. 3). Points of constant azimuth ( $\theta_0$ ) in the outside world map to vertical lines in the image plane. These vertical lines represent lines of constant  $\theta$  in the camera.

This mapping leads to the following expressions for the direction cosines of a ray that is incident on the mirror:

$$b_x = \cos \phi_0 \cdot \sin \theta_0 \quad (15)$$

$$b_y = \cos(90^\circ - \phi_0) = \sin \phi_0 \quad (16)$$

$$b_z = \cos \phi_0 \cdot \cos \theta_0 \quad (17)$$

We seek a mirror profile that ensures that the azimuthal and elevational angles in the external world are proportional to the azimuthal and elevational angles in the camera. That is,  $\theta_0 = \alpha\theta$  and  $\phi_0 = \beta\phi$  where  $\alpha$  and  $\beta$  are the azimuthal and elevational

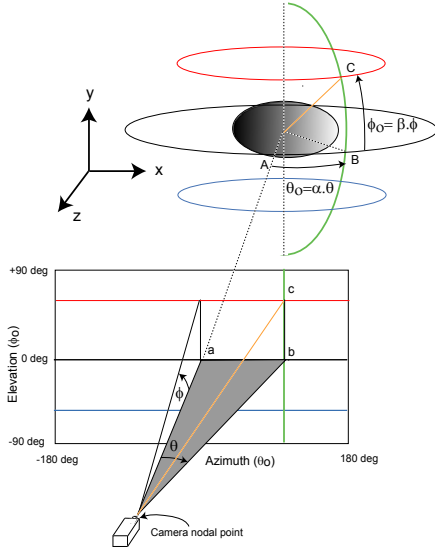


**Fig. 2** Configuration of equatorial view mirror

gains, respectively. Inserting these relationships into (15-17), we obtain the following expressions for the direction cosines of the reflected ray:

$$b_x = \cos \beta\phi \cdot \sin \alpha\theta \quad (18)$$

$$b_y = \sin \beta\phi \quad (19)$$

$$b_z = \cos \beta\phi \cdot \cos \alpha\theta \quad (20)$$

$$\text{where } \phi = \tan^{-1}\left(\frac{y}{z}\right) \quad (21)$$

and

$$\theta = \tan^{-1}\left(\frac{x}{z}\right) \quad (22)$$

The solution to the required mirror surface,  $f(x, y)$ , is obtained by incorporating (21) and (22) into (18) - (20), and inserting the resulting expressions for  $b_x, b_y$ , and  $b_z$ , as well as the expressions for  $a_x, a_y$ , and  $a_z$  into (12) and (13). Equations (12) and (13) are then integrated numerically, with respect to  $x$  and  $y$ , respectively, after specifying the boundary conditions at a particular point.

Typically, the boundary conditions would specify the distance of a point on the surface from the nodal point of the camera, and the orientation of the surface at that

point. For example, one could specify the distance  $r_0$  between the camera's nodal point and the surface along the camera's optical axis, and constrain the surface to be perpendicular to the optical axis at this point. That is,  $f(0,0) = r_0$  and  $p_x = 0, p_y = 0$  and  $p_z = 1$  at  $(x = 0, y = 0)$ . Using these boundary conditions, the profiles of the mirror along the  $x$  and  $y$  axes can be computed by integrating equations (12) and (13) with respect to  $x$  and  $y$ , respectively. We then compute the solution to the surface at other points  $(x, y)$ . This can be done in two ways: a) Integrate (12) along the  $x$  axis by using each previously computed value along the  $y$  axis, in turn, as a boundary condition; or b) integrate (13) along the  $y$  axis by using each previously computed value along the  $x$  axis, in turn, as a boundary condition.

It turns out that the surfaces derived using these two different procedures are not the same (details are not shown here due to lack of space). A ray tracing exercise reveals that neither surface satisfies the mapping properties that are required of the mirror. This finding indicates that there is no smooth surface that will achieve the desired mapping. The reason is that the local surface orientation that is required to produce the correct mapping at each point is, in general, different from the orientation of the global surface profile at that point.

The above problem can be overcome, however, by allowing the surface to be discontinuous. Such a solution is illustrated by the mirror portrayed in Fig. 3, whose shape has been derived using the following procedure: (i) compute the profiles along the  $x$  and  $y$  axes as described above; (ii) compute the profiles of cross sections perpendicular to the  $x$  axis by integrating equn (13) and using the values of the profile along the  $x$  axis as the initial conditions for successive profiles; (iii) determine the local slope along the  $x$  axis of the surface between successive cross sections by using equn (12). The resulting mirror profile is a surface that consists of a number of strips, or "ribbons" that are continuous along  $y$ , but display sawtooth-like discontinuities along  $x$ . The sawtooth-like profiles are especially prominent at the corners of the mirror, where  $\theta$  and  $\phi$  are large.

That this surface does indeed produce the desired mapping is illustrated in Fig. 5. This figure shows the relationship between the directions  $\theta_0$  and  $\phi_0$  of the rays that impinge upon the mirror, and the directions  $\theta$  and  $\phi$  of the corresponding rays that enter the camera, for 2500 points on the mirror surface. The ray-tracing was performed using a program written in Matlab (v. 6.5). It is clear that  $\theta_0$  is linearly related to  $\theta$ , and that the slope of this relationship agrees with the desired value of  $\alpha = 5$ . Similarly,  $\phi_0$  is

linearly related to  $\phi$ , and the slope of this relationship corresponds to the desired value of  $\beta = 3$ . Thus, the mirror achieves the desired mapping.

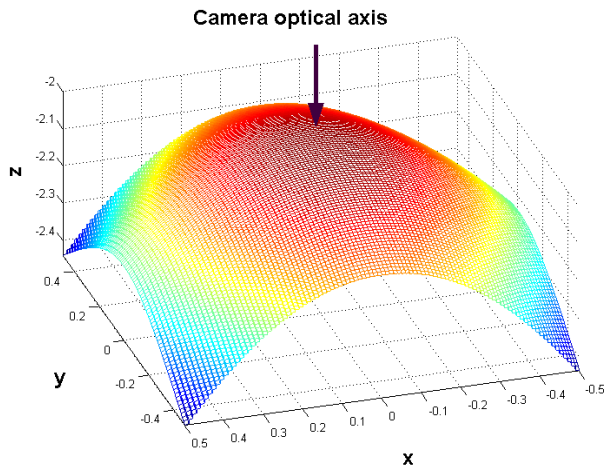


**Fig. 3** Solution for equatorial view mirror

The operation of the mirror is analogous, in some ways, to the operation of a Fresnel lens, which also possesses a sawtooth-like surface profile. In the case of the lens, light rays are refracted rather than reflected. But there, again, the local surface orientation that is required to refract the ray in the correct direction is different from the global orientation of the surface profile, leading to the discontinuities.

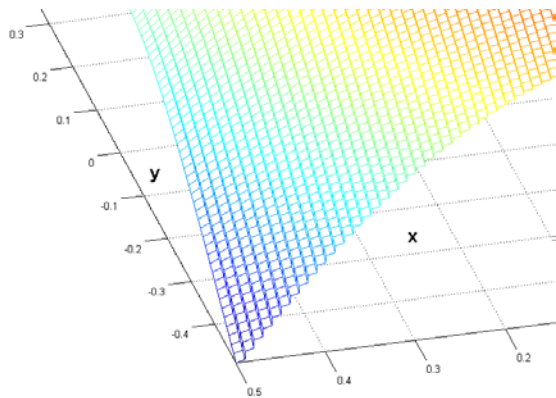


**Fig. 4** Close-up view of mirror of Fig. 3

The performance of the mirror of Fig. 3 is shown in Figs. 6-8, using a ray-tracing environment created through POV-Ray. Fig. 6 shows an object that was designed to test the mapping produced by the mirror. It consists of 12 vertically oriented rings, each of radius 300 units and thickness 30 units, separated in azimuth by 30 deg. They constitute reference longitudes in a viewsphere. There are also 5 horizontal rings, separated by an elevational angle of 30 deg. They provide reference latitudes in the viewsphere.

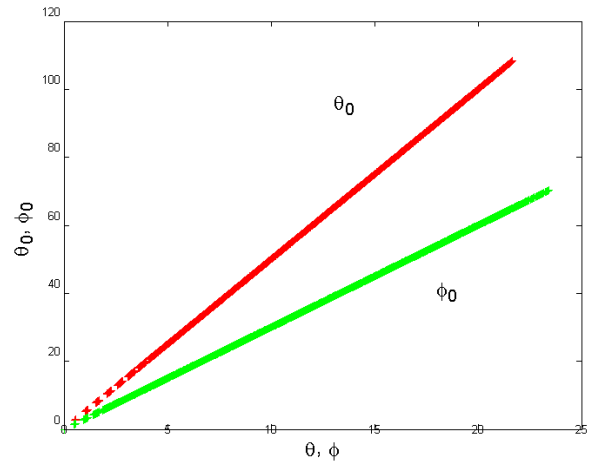


**Fig. 5** Illustration of mapping properties of equatorial view mirror shown in Fig. 3

The mirror is placed with its apex at the centre of the viewsphere. A pinhole camera, with a visual field of 70 deg (horizontal) by 50 deg (vertical) is positioned facing the mirror with its nodal point 1 unit from the apex. The camera-mirror system is located at the position indicated by the white sphere in the center of the ring framework.

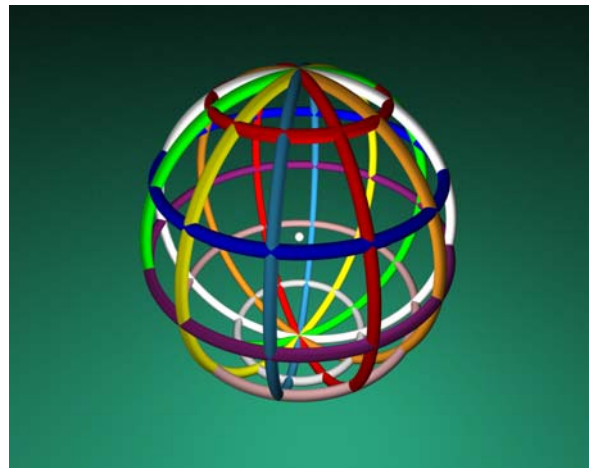


**Fig. 6** Standard object used in a ray-tracing environment to test imaging properties of the mirrors.

The image registered by the camera is shown in Fig. 7. It is clear that the image reflected by the mirror achieves the desired mapping. The longitudinal rings map into vertical columns, representing lines of constant azimuth ( $\theta_0$ ). The latitude rings map into horizontal rails that represent lines of constant elevation ( $\phi_0$ ). The images of the longitudinal rings become wider with increased elevation. This is as it should be, because, although the rings are of uniform thickness, their azimuthal subtense increases as the elevation of view is increased, approaching a value of 30 deg near the top of the viewsphere where the rings intersect.

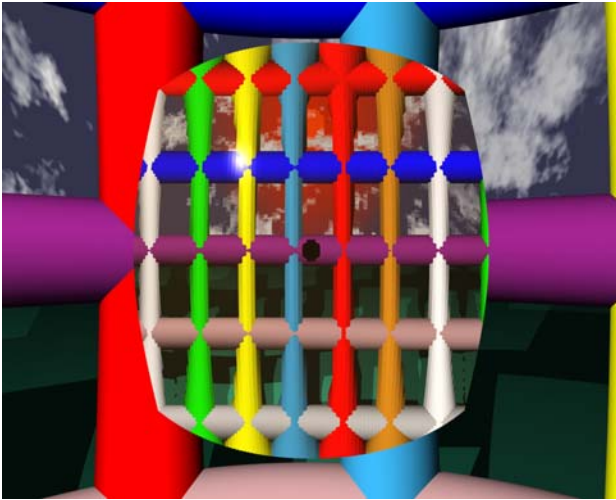


**Fig. 7** Wide-angle image captured by equatorial view mirror of Fig. 3

This mirror captures a total azimuthal field of ca. 210 deg and a total elevational field of ca. 150 deg. The dark disc in the centre of the image represents the reflection of the camera. The wide-angle imaging capacity of the mirror is illustrated by a comparison of Fig. 7 and 8, where Fig. 8 shows a camera image of the same scene acquired without the use of the mirror.

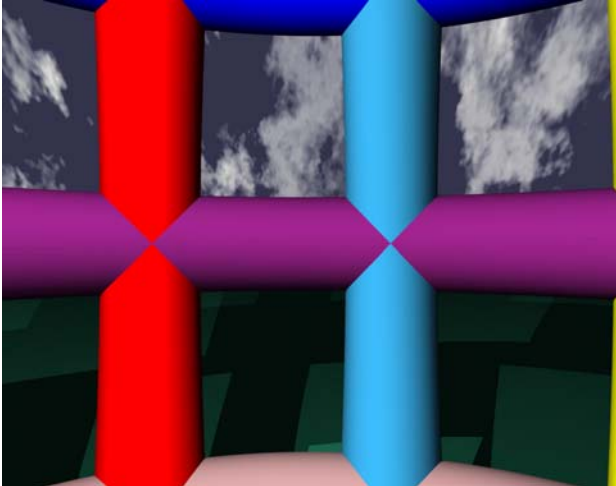


**Fig. 8** Camera image of test object without the use of a mirror

#### Narrow-angle imaging

In the above example the mirror gains ( $\alpha$  and  $\beta$ ) were greater than unity, thus enabling wide-angle imaging (i.e. enabling the camera to capture a larger segment of the world than it normally does). The opposite effect – narrow angle imaging – can be achieved by selecting values of  $\alpha$  and  $\beta$  that are lower than 1. Fig. 9 shows an example of a mirror surface with gains

$\alpha = 0.4$  and  $\beta = 0.6$ . Interestingly, the solution surface exhibits no discontinuities when the gains are both lower than unity. The right-hand panel shows the image captured by this surface. The result is a mirror that has the same qualitative mapping properties as the mirror in Fig. 3, but which magnifies rather than minifies.

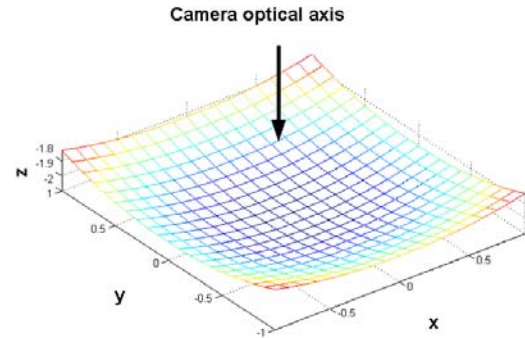


**Fig. 9** Profile of a mirror in which the azimuthal and elevational gains are less than unity

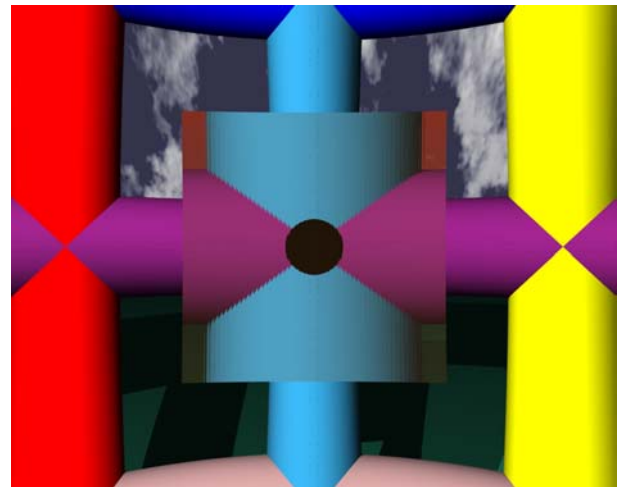


**Fig. 10** Image captured by mirror of Fig. 9

#### B. Polar view mirrors

The configuration of this class of mirrors is illustrated in Fig. 11. Here, the desired mapping is one in which the optical axis of the camera coincides with the polar axis of the viewsphere. With this configuration, points of constant elevation ( $\phi_0$ ) in the outside world map to lines that are parallel to the  $z$  axis in the image plane. These lines represent lines of constant  $\phi$  in the camera (Fig. 11). Points of constant azimuth ( $\theta_0$ ) in the outside world map to lines that are parallel to the  $x$  axis in the image plane. These horizontal lines represent lines of constant  $\theta$  in the camera. This mapping leads to the following constraints for the d.c.'s of a ray that is incident on the mirror:

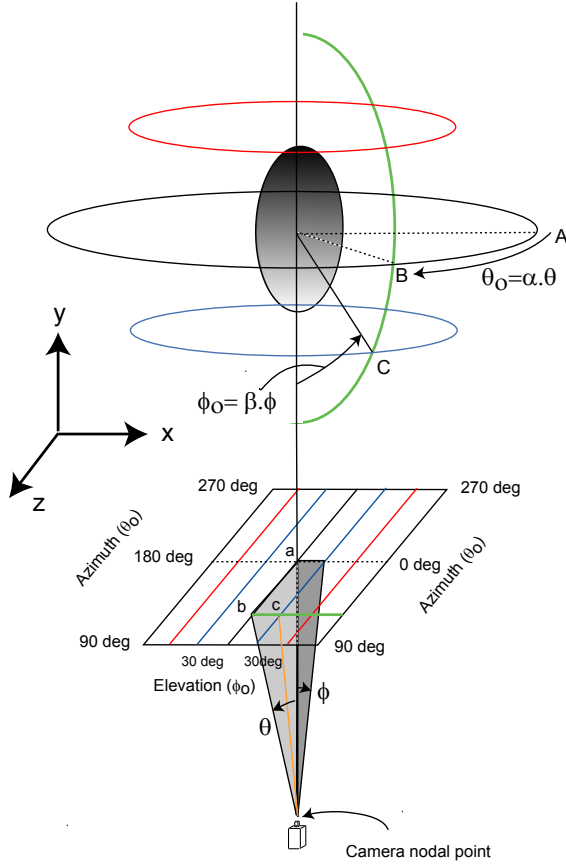


**Fig. 11** Configuration of polar view mirror

$$b_x = \sin \phi_0 \cdot \cos \theta_0 \quad (26)$$

$$b_y = -\cos \phi_0 \quad (27)$$

$$b_z = \sin \phi_0 \cdot \sin \theta_0 \quad (28)$$

We require that  $\theta_0 = \alpha \cdot \theta$  and  $\phi_0 = \beta \cdot \phi$  where  $\alpha$  and  $\beta$  are the azimuthal and elevational gains, respectively (see Fig. 11). Inserting these relationships into (26-28) we obtain the following expressions for the direction cosines of the reflected ray:

$$b_x = \sin \beta \phi \cdot \cos \alpha \theta \quad (29)$$

$$b_y = -\cos \beta \phi \quad (30)$$

$$b_z = \sin \beta \phi \cdot \sin \alpha \theta \quad (31)$$

Denoting the profile of the mirror surface by  $y = g(x, z)$ , we apply the boundary conditions  $g(0, 0) = r_0$ , where  $r_0$  is the distance of the surface from the nodal point of the camera at  $(0, 0)$ , and  $p_x = 0, p_z = 0$  and  $p_y = -1$  at  $(x = 0, z = 0)$ . The surface is computed by integrating equations (12)

and (13) as before, using the expressions (29-31) for  $b_x, b_y$  and  $b_z$ .

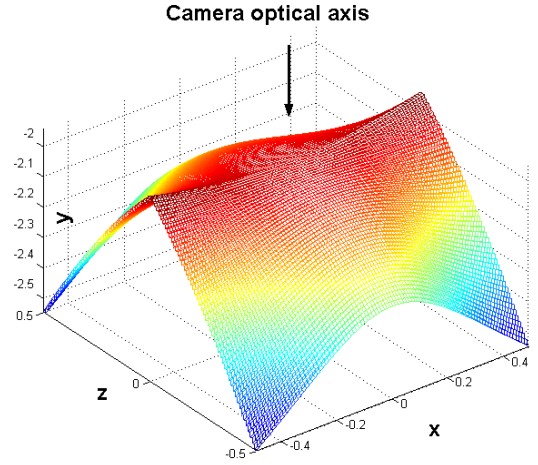


**Fig. 12** Profile of polar view mirror

The profile for a surface with  $\alpha = 5.0$ ,  $\beta = 5.0$  and  $r_0 = 1$  is shown in Fig. 12. A close-up view is shown in Fig. 13. Polar-view mirrors are also serrated near the corners. The imaging properties of this mirror are illustrated in Fig. 14. With this particular mirror, the left half of the image captures an azimuthal sector of ca. 210 deg, and the right half captures a symmetrical sector on the other side (there is some overlap in the azimuthal views at the upper and lower ends of the image). The mirror captures an elevation of ca. 100 deg on either side. The maximum elevation can be increased, if desired, by increasing the value of  $\beta$ .

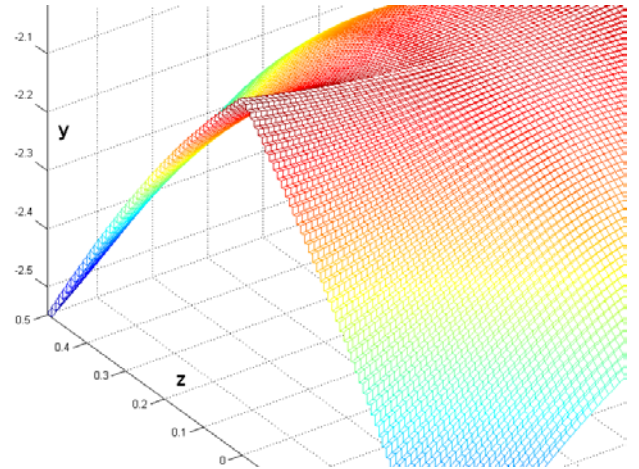


**Fig. 13** Close-up view of mirror of Fig. 12

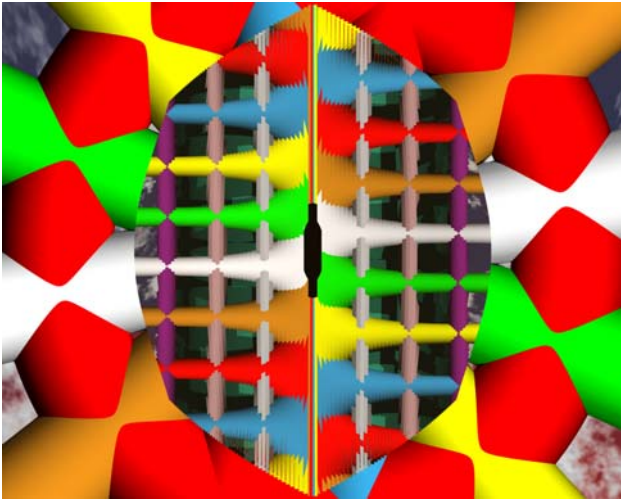


**Fig. 14** Wide-angle image captured by polar view mirror of Fig. 12

### Conclusions and future work

This paper has presented the design of a class of mirrors that (a) perform wide-angle imaging and (b) produce an image that represents the world in a Cartesian co-ordinate system in which the abscissa represents azimuth and the ordinate represents elevation. The disadvantages of these mirrors are (i) their manufacture can be somewhat complex, given the serrated nature of the profiles (except for the minifying mirrors, which possess a smooth surface), and (ii) the presence of the serrations could degrade image quality. The advantages of these mirrors are (i) direct optical unwarping, thus eliminating the need for a computer; (ii) the Cartesian mapping achieves uniform resolution in azimuth and elevation (a constant number of pixels per degree of azimuth or elevation, anywhere in the image) and (iii) the mapping makes full use of the camera's imaging plane (there are no unused corners, unlike the situation with the circular images captured by conventional conical imaging mirrors).

Future work will involve the construction of prototypes to assess image quality under real conditions, and to measure parameters of performance such as resolution and depth of field.

### References

- [1] Y. Yagi, S. Kawato and S. Tsuji. Real time omnidirectional image sensor (copis) for vision-guided navigation. *IEEE Transactions on Robotics and Automation*, 10: 11-22, 1994.
- [2] J.S. Chal and M.V. Srinivasan. Reflective surfaces for panoramic imaging. *Applied Optics*, 36 (31): 8275-8285, 1997.
- [3] M. Ollis, H. Herman and S. Singh. Analysis and design of panoramic stereo vision using equi-

- angular pixel cameras. Tech. Report CMU-RI-TR-99-04, Carnegie Mellon University, Pittsburgh, Pennsylvania, 1999.
- [4] S. Nayar. Catadioptric omnidirectional camera. *Proceedings, IEEE Conference on Computer Vision and Pattern Recognition*, 482-488, 1997.
- [5] R. A. Hicks and R. Bajcsy. Catadioptric sensors that approximate wide-angle perspective projections. *Proceedings, IEEE Workshop on Omnidirectional Vision*, Hilton Head Island, South Carolina 97-103, 1999.
- [6] R. Benosman, E. DeForas and J. Devars. A new catadioptric sensor for the panoramic vision of mobile robots. *Proceedings, IEEE Workshop on Omnidirectional Vision*, Hilton Head Island, South Carolina 112-116, 1999.
- [7] L.M. Kells. *Analytic Geometry and Calculus*. Prentice Hall, Inc., p. 441-442, 963.